

# **PREDICTING THE BURNING OF WOOD USING AN INTEGRAL MODEL**

by

**M. J. Spearpoint and J. G. Quintiere  
Department of Fire Protection Engineering  
University of Maryland  
College Park, MD 20742 USA**

**Reprinted from the Combustion and Flame, Vol. 123, No. 3, 308-325, November 2000.**

**NOTE: This paper is a contribution of the National Institute of Standards and Technology and is not subject to copyright.**



**NIST**

**National Institute of Standards and Technology**  
Technology Administration, U.S. Department of Commerce

# Predicting the Burning of Wood Using an Integral Model

M. J. SPEARPOINT\* and J. G. QUINTIERE

Department of Fire Protection Engineering, University of Maryland, College Park, MD 20742

This paper experimentally and theoretically examines the horizontal burning of four species of wood exposed to incident heat fluxes of 25–75 kW/m<sup>2</sup> with their grain oriented either parallel or perpendicular to the incident heat flux. Mass loss, temperatures, and char fractions were measured. A one-dimensional integral model that describes the transient pyrolysis of a semi-infinite charring solid subject to a constant radiant heat flux was developed. The solutions to the integral model for the burning rate were compared with data using analytical short-time and long-time solutions. Reasonable comparative results are shown for mass loss rate, surface temperature, char depth, and effective thermal penetration. © 2000 by The Combustion Institute

## NOMENCLATURE

$\alpha$	thermal diffusivity [m <sup>2</sup> /s], absorptivity [–]
$\beta$	ratio of convective gain and radiative loss with incident heat flux [–]
$c$	specific heat [J/kg · K]
$\delta$	depth [m]
$\Delta$	dimensionless depth [–]
$\phi$	char fraction [–]
$h_c$	heat transfer coefficient [W/m <sup>2</sup> · K]
$h$	enthalpy [J]
$\Delta H_v$	heat of vaporization [J/kg], see Eq. 17
$l$	thermal inertia, $k\rho c$ [J <sup>2</sup> · m <sup>-4</sup> · K <sup>-2</sup> · s <sup>-1</sup> ]
$k$	thermal conductivity [W/m · K]
$L$	heat of gasification [J/kg], Eq. 39
$m$	mass [kg]
$M$	dimensionless mass loss rate [–]
$q$	heat flux [W/m <sup>2</sup> ]
$\rho$	density [kg/m <sup>3</sup> ]
$T$	temperature [°C] or [K]
$\theta$	dimensionless temperature [–]
$t$	time [s]
$\tau$	dimensionless time [–]
$\sigma$	Stefan-Boltzmann constant [W/m <sup>2</sup> · K]

## Subscripts

$0$	initial, ambient
$c$	convective
$cr$	critical
$\phi$	char
$f$	final
$fl$	flame
$g$	gas
$i$	incident

$ig$	ignition
$P$	pressure
$s$	surface or steady when subscripted to $\delta$
$v$	vaporization
$w$	virgin wood

## Superscripts

$(\cdot)^{\prime\prime}$	per unit area
$(\cdot)^{\prime}$	per unit time

## INTRODUCTION

Ever since prehistoric times humans have known that wood burns, and the ability of wood to burn has been both a benefit and a problem. The capability to predict the burning rate of wood in modern times has become increasingly important as fire safety engineering moves toward a performance-based approach to building design and as the need to protect the environment through forest fire containment and bio-mass incineration increases.

The purpose of this paper is to examine the burning rate behavior of wood and compare those results to a one-dimensional integral model for charring materials. The experimental data used in this paper are taken from the work by Spearpoint [1] in which the ignition and burning rate of several species of wood were measured in the Cone Calorimeter [2], a standard apparatus to measure the mass loss rate and energy release rate of radiant heated materials.

The pyrolysis behavior of solid materials can be divided into two types: noncharring and charring. Noncharring materials burn away

\*Corresponding author. E-mail: mike@civil.canterbury.ac.nz

completely, leaving no residue, and can be modeled using theory similar to flammable liquids. In contrast, charring materials leave relatively significant amounts of residue when they burn. The pyrolysis of charring materials such as wood is a complex interplay of chemistry, heat, and mass transfer. Charring materials must be modeled in terms of a pyrolysis front penetrating into the material with an increasing surface temperature and without a well-defined steady state.

Consider a "thick" sample of wood with its surface uniformly exposed to a constant external incident heat flux and a source of ignition (a pilot) close by such that the heat and mass transfer through the sample can be considered one-dimensional. The incident flux pyrolyzes the wood, releasing volatile fuel gases with a mass flow rate that depends on the intensity of the incident energy and the orientation of the grain. The mass flow rate of the volatiles must exceed the lower flammable limit of the fuel/air mixture for piloted ignition to occur. Ignition can occur at surface temperatures anywhere from 200°C up to 400°C. At the instant of ignition, the heat flux to the surface of the wood is a combination of the external flux plus the flux from the flame. The rate of heat release rapidly rises to a maximum, then a char layer gradually builds up as the pyrolysis front moves inward. The char layer forms an increasing thermal resistance between the exposed surface and the pyrolysis front, resulting in a continuously decreasing rate of heat release after the first peak. If the sample is sufficiently thick, it is found in experiments [3] that its rate of heat release eventually reaches a more or less steady value.

At temperatures above around 300°C the char layer begins to break down rapidly [3]. The char layer also shrinks and pressure gradients are set up within the material. Small cracks appear on the surface, and these cracks allow volatiles to escape more easily. The cracks gradually widen as the char layer deepens, leading to characteristic "alligatoring" patterns. The charring rate of wood is also very sensitive to the presence of inorganic impurities, such as fire retardants, because they affect the chemical kinetics of the pyrolysis process [4].

After the volatiles have been exhausted, flam-

ing ceases and a solid char residue remains. The char continues to burn in a smoldering mode. Prior to that, char oxidation is usually minimal since the flame prevents diffusion of oxygen to the surface. Therefore, heat release rate and related quantities measured during the flaming phase are predominantly those of the volatiles. However, for a period both surface oxidation and discrete surface flamelets at the wood cracks can coexist.

The main constituent of wood char is carbon, and the net heat of combustion for a carbon and oxygen to carbon dioxide reaction is approximately 32 MJ/kg. As noted by Janssens [3], the average net heat of combustion of wood for a complete reaction is 17 MJ/kg. For a typical char yield for dry wood of 33% of the original mass, the mean heat of combustion during the flaming mode  $\Delta H_{f,w}$  can be found by solving

$$\frac{1}{3}(32) + \frac{2}{3}(\Delta H_{f,w}) = 17 \quad (1)$$

which gives a value of about 10 MJ/kg of volatiles. Thus, only about 60% of the energy of wood is released during the flaming stage of combustion.

## PREVIOUS STUDIES

### General

There is a substantial volume of work regarding the ignition, pyrolysis, burning, and charring behavior of wood (and cellulosic materials). It is not the intent of this work to give a thorough review, but a brief summary will be presented.

Kanury [5] gives a general overview of the ignition of solids by thermal radiation or convection. Roberts [6] reviewed the role of kinetics for the pyrolysis of wood and related materials. Simms [7] examined the role of thermal radiation on the damage to cellulosic solids by considering the chemical and thermal histories of the material. Work on char rate in wood includes studies by Kanury [8] who examined the phenomenon using Arrhenius pyrolysis kinetics. A detailed study of the pyrolysis kinetics of cellulose has been conducted by Suuberg et al. [9].

Atreya and coworkers have done extensive work on the ignition and burning of wood. In his

initial work Atreya [10] included experimental observations for the piloted ignition of wood and identified several important factors including: pyrolysis of wood produces gaseous fuels and inerts; diffusion and mixing of the fuel and ambient air, which produces a flammable gas in the boundary layer; premixed flame ignition by a pilot source; quenching by the surface and establishment of a sustained diffusion flame after the premixed flame has vanished. Further work by Atreya et al. [11] examined the effect of sample orientation on piloted ignition and flame spread on wood.

### Ignition and Burning Rate Models

Several models for the burning rate of solid materials, both charring and noncharring, have been developed. Examples include the studies by Chen et al. [12], Wichman and Atreya [13], Yuen et al. [14], and Parker [15]. These models range from simple treatments of the ignition and burning process using pure heat conduction models to the use of complex chemical kinetics for the pyrolysis of a charring material. Many of the models consist of complex computational codes that require a relatively large number of difficult-to-obtain property values to complete their predictions.

In this paper, we examine the integral model initially developed by Quintiere [16]. A one-dimensional pyrolysis model which includes the processes of charring, vaporization, flame, and heat conduction effects was proposed. This model was applied by Quintiere and Iqbal [17] to the gasification of a noncharring material. Anderson [18] validated the integral approach with some exact solutions. Finally, in a study by Hopkins et al. [19, 20] the model was compared against experimental data for the burning of noncharring thermoplastics.

A nearly identical integral model for the burning of a charring material was also successfully demonstrated by Moghtaderi et al. [21] by validation with an exact numerical solution and with experimental data. Our analytical short- and long-time solutions are a new contribution, along with the data for four wood species and the effect of grain orientation.

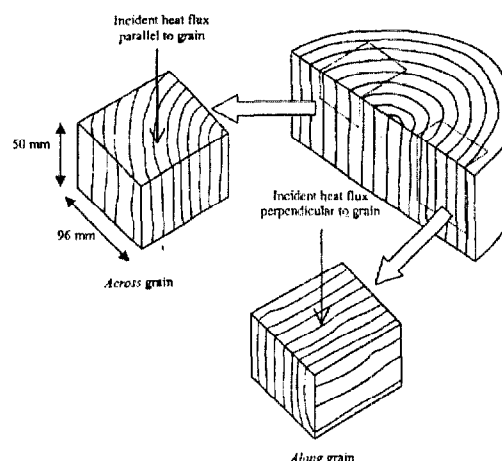


Fig. 1. Sample grain configurations.

### DESCRIPTION OF EXPERIMENT

The wood samples were provided such that the grain was parallel to the incident heat flux (i.e., cut *across* the grain) and perpendicular to the incident heat flux (i.e., cut *along* the grain) as shown in Fig. 1. Four species of wood were studied: Douglas fir, redwood, red oak, and maple. Douglas fir and redwood are both softwoods whereas red oak and maple are both hardwoods. The samples were all cut from the sapwood portion of sections of lumber and were nominally 50 mm thick by 96 mm square.

Samples were stored in a desiccator at nominally 50% relative humidity and 20°C. The moisture content of each sample was measured prior to exposure. All samples were tested in the Cone Calorimeter in the horizontal orientation. Samples were wrapped in a single layer of aluminum foil and placed into a 50-mm-high sample holder.

The main "burning rate" series of 54 tests were conducted at the University of Maryland by the authors to support a related study by Schroeder [23]. The tests included the measurement of time to ignition, mass loss, rate of heat release, and smoke extinction data. Incident heat fluxes of 25 kW/m<sup>2</sup>, 35 kW/m<sup>2</sup>, 50 kW/m<sup>2</sup>, and 75 kW/m<sup>2</sup> were selected for these experiments. For the majority of the burning rate tests, exposure times of 25 minutes were used; however, in a few cases the exposure time was extended to 75 minutes. A total of 41 additional

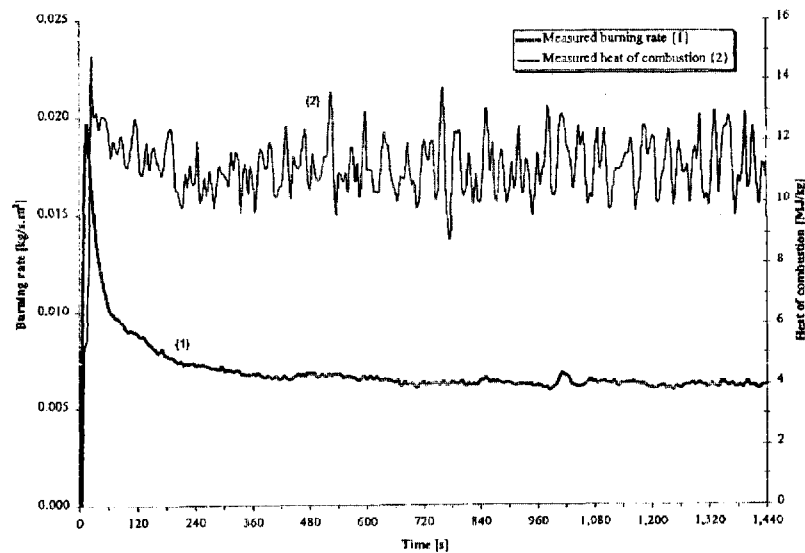


Fig. 2. Typical burning rate and heat of combustion data (Douglas fir, along grain,  $75 \text{ kW/m}^2$  for 25 minutes).

“ignition only” tests at lower heat fluxes were conducted; a more detailed description of these tests and analysis of the data is given elsewhere by Spearpoint [1].

For the majority of the “burning rate” tests, 0.813-mm (0.032”)-diameter sheathed Type K thermocouples were inserted halfway into the samples through horizontal holes drilled at heights of 4 mm, 12 mm, 24 mm, and 36 mm below the top surface. A thermocouple was located between the back of the sample and the retainer frame (i.e., at 50 mm). Figures 2 and 3 show typical results obtained from the tests. The more rapid increase in the temperature mea-

sured by the 50-mm thermocouple is due to the retainer frame heating up as it is exposed to the external heat flux. The endothermic effect of moisture in the wood is clearly indicated at  $100^\circ\text{C}$ .

## THEORY

### Assumptions

Features of the integral model and the physics of the thermal decomposition of wood are portrayed in Fig. 4. Specific assumptions include:

- The fuel decomposes to gaseous fuel (volatiles) and char in an infinitesimal pyrolysis front at a fixed vaporization temperature.
- The solid is infinitely thick.
- The virgin wood is inert up to ignition and decomposition.
- The char material is also inert.
- The flame heat flux remains constant.
- The density of the volatiles is much less than the density of the virgin wood and the char.
- Material properties are constant over the range of temperatures considered.
- The volatiles do not accumulate within the char layer but are produced and exit immediately.

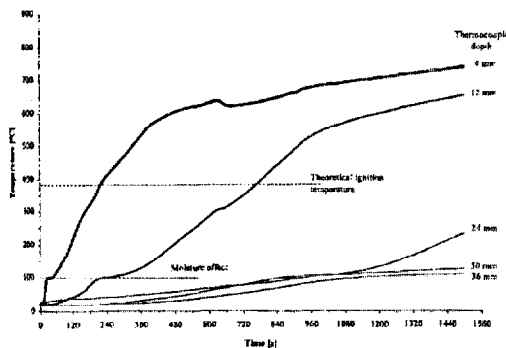


Fig. 3. Typical thermocouple data (Douglas fir, along grain,  $75 \text{ kW/m}^2$  for 25 minutes).

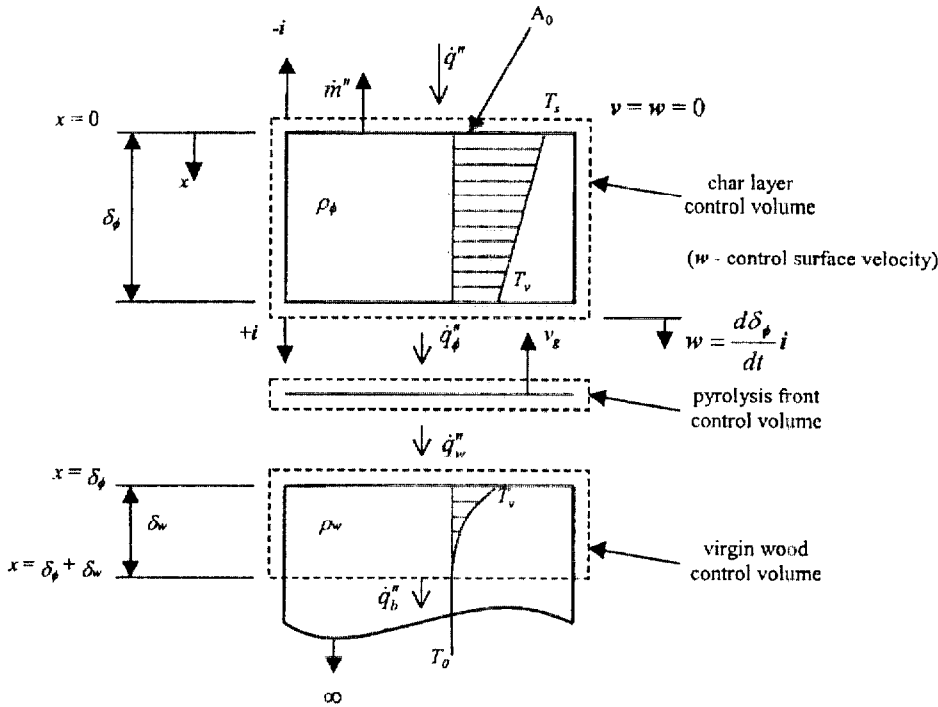


Fig. 5. Burning rate model control volumes.

convection, the net heat flux at a given time \$t\$ is given by

$$\dot{q}''(t) = \alpha \dot{q}''_i - \epsilon \sigma (T_s^4 - T_0^4) - h_c (T_s - T_0). \quad (4)$$

Thus, just before ignition when \$t = t\_{ig}^-\$, and assuming the surface emissivity \$\epsilon\$ and the absorptivity \$\alpha\$ are 1, from Eq. 4

$$\dot{q}''(t_{ig}^-) = \dot{q}''_- = \dot{q}''_i - \sigma (T_{ig}^4 - T_0^4) - h_c (T_{ig} - T_0). \quad (5)$$

Just after ignition, when \$t = t\_{ig}^+\$, from Eq. 3

$$\dot{q}''(t_{ig}^+) = \dot{q}''_+(T_{ig}) = \dot{q}''_b + \dot{q}''_i - \sigma (T_{ig}^4 - T_0^4). \quad (6)$$

Hence there is a step-change in the surface heat flux at ignition. Using the integral model, Spearpoint [1] has shown that the thermal penetration depth prior to ignition is given by

$$\delta = \sqrt{3 \frac{k_w}{\rho_w c_w} \left[ \frac{2 - \beta}{1 - \beta} \right] t} \quad (7)$$

where

$$\beta \equiv \frac{\sigma (T_s^4 - T_0^4) + h_c (T_s - T_0)}{\dot{q}''_i} \quad (8)$$

and the time to ignition can be obtained from

$$t_{ig} = \frac{4}{3} k_w \rho_w c_w \left[ \frac{1 - \beta_{ig}}{2 - \beta_{ig}} \right] \frac{(T_{ig} - T_0)^2}{[\dot{q}''_i]^2} \quad (9)$$

where

$$\beta_{ig} \equiv \frac{\sigma (T_{ig}^4 - T_0^4) + h_c (T_{ig} - T_0)}{\dot{q}''_i} = \frac{\dot{q}''_{cr}}{\dot{q}''_i}. \quad (10)$$

### Conservation Equations

The decomposition of the charring material is split into three control volumes; (1) the char layer, (2) the pyrolysis front, and (3) the virgin material (Fig. 5). The char matrix contains solid char and fuel gases. The mass flux of the escaping volatiles is given as

$$\dot{m}'' = \rho_g v_g. \quad (11)$$

Considering conservation of energy for the char layer we obtain

$$\begin{aligned} (\rho_g c_g + \rho_\phi c_\phi) \frac{d}{dt} \int_0^{\delta_\phi} (T - T_v) dx + \dot{m}'' c_g (T_s - T_v) \\ = \dot{q}''_+(T_s) - \dot{q}''_\phi + p(T_v) \frac{d\delta_\phi}{dt}. \end{aligned} \quad (12)$$

Typically  $\rho_g c_g \ll \rho_\phi c_\phi$  since  $\rho_g \approx 1 \text{ kg/m}^3$  and  $c_g \approx 1 \text{ kJ/kg} \cdot \text{K}$  while  $\rho_\phi \approx 200 \text{ kg/m}^3$  [25] and  $c_\phi \approx 1.3 \text{ kJ/kg} \cdot \text{K}$  [26]. In addition, we assume that  $\rho_\phi c_\phi (T - T_v) \gg p(T_v)$ , since as an order of magnitude estimate  $(T - T_v) \gg 100 \text{ K}$ , thus  $\rho_\phi c_\phi (T - T_v) \approx 2.6 \times 10^4 \text{ kJ/m}^3$  or  $2.6 \times 10^7 \text{ N/m}^2$  but typically  $p \approx 10^5 \text{ N/m}^2$ . Thus Eq. 12 can be simplified to

$$\begin{aligned} \rho_\phi c_\phi \frac{d}{dt} \int_0^{\delta_\phi} (T - T_v) dx + \dot{m}'' c_g (T_s - T_v) \\ = \dot{q}''_+(T_s) - \dot{q}''_\phi. \end{aligned} \quad (13)$$

Using conservation of mass on the pyrolysis front control volume, we obtain

$$(\rho_w - \rho_\phi - \rho_g) \frac{d\delta_\phi}{dt} = \rho_g v_g. \quad (14)$$

Substituting Eq. 11 into Eq. 14 and assuming the density of the gas is small,

$$(\rho_w - \rho_\phi) \frac{d\delta_\phi}{dt} = \dot{m}''. \quad (15)$$

Similarly, using conservation of energy for the pyrolysis front

$$\begin{aligned} \rho_w \frac{d\delta_\phi}{dt} \left[ \{h_g(T_v) - h_w(T_v)\} \right. \\ \left. - \frac{\rho_\phi}{\rho_w} \{h_g(T_v) - h_\phi(T_v)\} \right] \\ = \dot{q}''_\phi - \dot{q}''_w. \end{aligned} \quad (16)$$

Based on the mass of the virgin wood, we define the heat of vaporization as energy required to convert the solid to char and fuel vapor per unit mass of original solid such that

$$\begin{aligned} \Delta H_v \equiv \{h_g(T_v) - h_w(T_v)\} \\ - \frac{\rho_\phi}{\rho_w} \{h_g(T_v) - h_\phi(T_v)\}, \end{aligned} \quad (17)$$

then Eq. 16 becomes

$$\rho_w \frac{d\delta_\phi}{dt} [\Delta H_v] = \dot{q}''_\phi - \dot{q}''_w. \quad (18)$$

Finally, by conservation of energy for the virgin wood control volume and assuming negligible heat loss to the back, we obtain

$$\begin{aligned} \rho_w c_w \frac{d}{dt} \int_0^{\delta_\phi} [T(x', t) - T_0] dx' \\ + \rho_w c_w \frac{d\delta_\phi}{dt} (T_v - T_0) \\ = \dot{q}''_w \end{aligned} \quad (19)$$

where  $x = x' + \delta_\phi$ .

### Temperature Profiles and Governing Equations

The temperature profile in the char layer is assumed to be linear function with depth such that

$$T - T_v = (T_s - T_v) \left(1 - \frac{x}{\delta_\phi}\right) \quad (20)$$

satisfying boundary conditions  $T = T_s$  at  $x = 0$  and  $T = T_v$  at  $x = \delta_\phi$ . The temperature profile in the virgin wood is assumed to be a second-order function of depth such that

$$T - T_0 = (T_v - T_0) \left(1 - \frac{x'}{\delta_w}\right)^2 \quad (21)$$

satisfying boundary conditions  $T = T_v$  at  $x' = 0$ ,  $T = T_0$  at  $x' = \delta_w$ , and  $\partial T/\partial x = 0$  at  $x' = \delta_w$  (see Figs. 4 and 5). With these profiles, and using Eq. 15, Eq. 18 becomes

$$\frac{\dot{m}''}{(1 - \phi)} \Delta H_v = \frac{k_\phi (T_s - T_v)}{\delta_\phi} - \frac{2k_w (T_v - T_0)}{\delta_w}. \quad (22)$$

Similarly Eq. 13 becomes

$$\begin{aligned} \rho_\phi c_\phi \frac{d}{dt} (T_s - T_v) \delta_\phi + \dot{m}'' c_g (T_s - T_v) \\ = \dot{q}''_+(T_s) - \frac{k_\phi (T_s - T_v)}{\delta_\phi}. \end{aligned} \quad (23)$$

Finally Eq. 19 becomes

$$\frac{1}{3} \frac{d\delta_w}{dt} + \frac{\dot{m}''}{\rho_w(1-\phi)} = \frac{2(k_w/\rho_w c_w)}{\delta_w}. \quad (24)$$

Adding Eq. 23 and Eq. 22 we obtain

$$\begin{aligned} \frac{\rho_w c_w \phi}{2} \left( \frac{d}{dt} T_s - \frac{d}{dt} T_v \right) \delta_\phi + \dot{m}'' c_g (T_s - T_v) \\ + \frac{\dot{m}''}{(1-\phi)} [\Delta H_v] \\ = \dot{q}''_+(T_s) - \frac{2k_w(T_v - T_0)}{\delta_w}. \end{aligned} \quad (25)$$

If the time just after ignition is considered, then  $t = t_{ig}^+$  with  $T_s = T_v = T_{ig}$ ,  $\dot{m}'' = \dot{m}''_{ig}$  and  $\delta_w = \delta_{ig}$ . Thus, from Eq. 25, the burning rate at ignition is

$$\dot{m}''_{ig} = \frac{(1-\phi)}{\Delta H_v} \left[ \dot{q}''_+ - \frac{2k_w(T_{ig} - T_0)}{\delta_{ig}} \right]. \quad (26)$$

From Eqs. 5, 6, and 21 it can be shown that

$$\begin{aligned} \dot{m}''_{ig} &= \frac{(1-\phi)}{\Delta H_v} [\dot{q}''_+(T_s) - \dot{q}''_-] \\ &= \frac{(1-\phi)}{\Delta H_v} [\dot{q}''_f + h_c(T_{ig} - T_0)]. \end{aligned} \quad (27)$$

#### Dimensionless Analysis and Solutions

The following dimensionless variables were selected to consolidate the variables

$$M \equiv \frac{\dot{m}'' L}{(1-\phi)\dot{q}''_+(T_v)} \quad (28)$$

$$M_{ig} \equiv \frac{\dot{m}''_{ig} L}{(1-\phi)\dot{q}''_+(T_v)} \quad (29)$$

$$\delta_t \equiv \frac{2k_w L}{c_w \dot{q}''_+(T_v)} \quad (30)$$

$$\lambda \equiv \frac{\delta_w}{\delta_s} \quad (31)$$

$$\lambda_{ig} \equiv \frac{\delta_{ig}}{\delta_s} \quad (32)$$

$$\lambda_\phi \equiv \frac{\delta_\phi}{\delta_s} \quad (33)$$

$$\theta \equiv \frac{T}{T_v} \quad (34)$$

$$\theta_s \equiv \frac{T_s}{T_v} \quad (35)$$

$$\theta_0 \equiv \frac{T_0}{T_v} \quad (36)$$

$$\tau \equiv \frac{\alpha t}{\delta_s^2} \quad (37)$$

$$\tau_{ig} \equiv \frac{\alpha t_{ig}}{\delta_s^2} \quad (38)$$

where  $\delta_s$  is a steady-state depth (for the non-charring case). The heat of gasification per unit mass of virgin wood,  $L$ , is defined as

$$L \equiv \Delta H_v + c_w(T_v - T_0). \quad (39)$$

Substituting for the dimensionless variables in the four governing equations: Eqs. 15, 22, 23, and 24,

$$M = \frac{T_v c_w}{\Delta H_v} \left[ \left( \frac{k_\phi}{k_w} \right) \frac{1}{2} \frac{(\theta_s - 1)}{\Delta_\phi} - \frac{(1 - \theta_0)}{\Delta} \right] \quad (40)$$

$$\begin{aligned} \frac{1}{4} \phi \left( \frac{c_\phi}{c_w} \right) \frac{d}{d\tau} [(\theta_s - 1)\Delta_\phi] \\ + \left[ (1-\phi) \left( \frac{c_g}{c_w} \right) (\theta_s - 1) + \frac{\Delta H_v}{c_w T_v} \right] M \\ = \frac{L}{c_w T_v} \frac{\dot{q}''_+(T_s)}{\dot{q}''_+(T_v)} - \frac{(1 - \theta_0)}{\Delta} \end{aligned} \quad (41)$$

$$\frac{1}{3} \frac{d\Delta}{d\tau} + 2M = \frac{2}{\Delta} \quad (42)$$

$$M = \frac{1}{2} \frac{d\Delta_\phi}{d\tau}. \quad (43)$$

The variables  $M$ ,  $\Delta$ ,  $\Delta_\phi$ , and  $\theta_s$  must be determined from these ordinary differential equations with ignition as the initial condition. We now consider three phases of burning: (a) ignition, (b) a short time after ignition, and (c) a long time after ignition.

(a) Ignition, the initial condition,  $\tau = \tau_{ig}$

$$M = M_{ig} = \left( \frac{L}{\Delta H_v} \right) \left[ 1 - \frac{\dot{q}''_-}{\dot{q}''_+(T_v)} \right]. \quad (44)$$

From Eqs. 7 and 9

$$\Delta = \Delta_{ig} = \left[ \frac{c_w(T_{ig} - T_0)}{L} \right] \left[ \frac{\dot{q}_+''(T_{ig})}{\dot{q}_i''} \right]. \quad (45)$$

and

$$\Delta_\phi = 0 \quad (46)$$

$$\theta_s = 1 \quad (47)$$

(b) Short-time solution,  $\tau \approx \tau_{ig}$

Integrating Eq. 43 and given that  $M \approx M_{ig}$  at  $\tau_{ig}$  then

$$\Delta_\phi \approx 2M_{ig}(\tau - \tau_{ig}). \quad (48)$$

From Eq. 41, with no char,  $\Delta_\phi = 0$  and assuming  $T_s = T_v$ , thus  $\theta_s = 1$  and  $\dot{q}_+''(T_s) \rightarrow \dot{q}_+''(T_v)$  then

$$M = \frac{L}{\Delta H_v} \left[ 1 - \frac{c_w(T_v - T_0)}{L} \cdot \frac{1}{\Delta} \right]. \quad (49)$$

Since at early times  $\Delta - \Delta_{ig}$  is small,  $\tau - \tau_{ig}$  is small and  $e^x \approx 1 + x$  for small  $x$ , then from Eqs. 39, 42, and 49

$$\Delta \approx \Delta_{ig} + 6 \left( \frac{L}{\Delta H_v} \right) (1 - \Delta_{ig})(\tau - \tau_{ig}). \quad (50)$$

(c) Long-time solution,  $\tau \gg \tau_{ig}$

Finally consider times much later than the ignition time (i.e., long-time). Let the char depth rate approach zero,  $d\Delta_\phi/d\tau \rightarrow 0$ , the surface temperature approach a constant,  $d\theta_s/d\tau \rightarrow 0$ , and the burning rate tend to zero,  $M \rightarrow 0$ . Integrating Eq. 42

$$\Delta \approx \sqrt{\Delta_{ig}^2 + 12(\tau - \tau_{ig})}. \quad (51)$$

From Eqs. 41 and 3, as  $\Delta \rightarrow \infty$ , and assuming  $\theta_0^4$  is small, then

$$\theta_s \approx \left[ \frac{\dot{q}_+'' + \dot{q}_i''}{\sigma T_v^4} \right]^{1/4}. \quad (52)$$

From Eq. 40 assuming  $\theta_s$  is constant, the thermal penetration depth approaches infinity,  $\Delta \rightarrow \infty$ , as time tends to infinity,  $\tau \rightarrow \infty$  and finally at time  $\tau_{ig}$  the char depth  $\Delta_\phi = 0$ , then

$$\Delta_\phi \approx \sqrt{2 \left( \frac{c_w T_v}{\Delta H_v} \right) \left( \frac{k_\phi}{k_w} \right) (\theta_s - 1)(\tau - \tau_{ig})}. \quad (53)$$

and

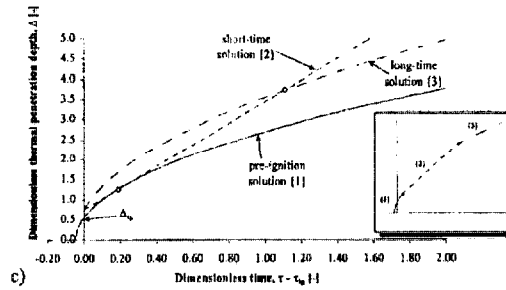
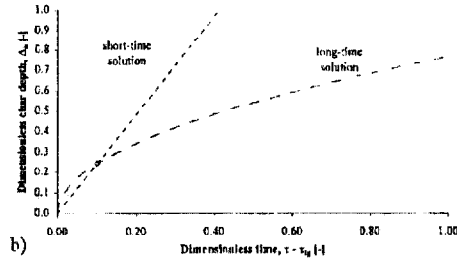
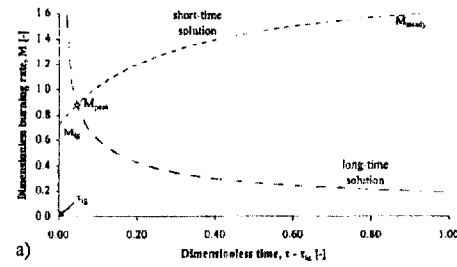


Fig. 6. General form of the dimensionless equations for the a) burning rate, b) char depth, and c) thermal penetration depth.

$$M \approx \sqrt{\frac{\left( \frac{c_w T_v}{\Delta H_v} \right) \left( \frac{k_\phi}{k_w} \right) (\theta_s - 1)}{8(\tau - \tau_{ig})}} \quad (54)$$

where it can be shown that  $k_\phi/k_w \approx \phi$ .

The general form of the dimensionless equations for the burning rate, thermal penetration depth, and char depth is shown in Fig. 6. The short-time burning rate solutions are equivalent to what would be obtained by a noncharring material as detailed by Hopkins [19]. At ignition the short-time burning rate starts at a given point after which it increases to a maximum steady-state value  $M_{steady}$ , where it remains. A real burning material would of course eventually consume all its fuel and the burning rate would drop to zero.

TABLE 1

Measured and Derived Properties of Wood Samples Tested

Species	Grain Orientation	Measured Average	Derived Critical	Derived Ignition	Derived Thermal	Derived Specific
		Density $\rho_w$ (kg/m <sup>3</sup> )	Heat Flux $\dot{q}''_c$ (kW/m <sup>2</sup> )	Temperature $T_{ig}$ (°C)	Conductivity $k_w$ (W · m <sup>-1</sup> · K <sup>-1</sup> )	Heat Capacity $c_w$ (J · kg <sup>-1</sup> · K <sup>-1</sup> )
Redwood	along	354	15.5	375	0.19	3200
	across	328	5.9	204	0.85	7400
Red oak	along	753	10.8	304	0.44	3100
	across	678	9.2	275	0.86	3200
Douglas fir	along	502	16.0	384	0.23	2200
	across	455	8.4	258	0.80	4000
Maple	along	741	13.9	354	0.35	2500
	across	742	3.8	150	2.08	7100

The long-time solution effectively starts from an infinite burning rate from where it decays toward zero. There is a transition point at which the short-time and long-time solutions cross. This point marks the peak burning rate  $M_{peak}$  and it is less than the steady-state noncharring material burning rate. Thus, for a charring material the burning rate follows the short-time solution up to the transition point (the peak burning rate) and thereafter follows the long-time solution. The long-time solution also eventually achieves an almost "steady" burning regime.

For the char depth, the short-time solution is a linear function; transition to the long-time solution is illustrated in Fig. 6. In the case of the thermal penetration depth there are three solutions to consider: the preignition, short-time, and long-time solutions. Figure 6 shows these three solutions in their complete form and, for clarity, the inset plot shows the three solutions with the nonapplicable portions of the curves removed.

#### THERMOPHYSICAL MATERIAL PROPERTIES

The integral model requires a number of properties to be obtained for the material. A few of the properties can be easily measured, others must be obtained from experimental data, and the remainder may be obtained from the literature. The properties needed depend on the model, and can be considered "effective" properties.

The model requires (among others) the thermal conductivity  $k$ , density  $\rho$ , and specific heat  $c$

and the related properties of thermal inertia  $I = k\rho c$  and thermal diffusivity  $\alpha = k/\rho c$ . Regarded as constant in the model, these properties will vary as the material undergoes thermal, mechanical, and chemical changes.

The density of the virgin wood was directly obtained by measurement and it was assumed that the thermal diffusivity remained constant. From the ignition data the integral model theory was used to obtain the ignition temperature  $T_{ig}$ , the specific heat, and the thermal conductivity. Table 1 summarizes the directly "measured" and experimentally "derived" properties for each species of wood in the two grain orientations.

In addition, we need to obtain estimates of the heat of gasification  $L$  and heat flux of the flame  $\dot{q}''_f$ . This determination was the most difficult. It was done on an iterative procedure with some judgment of "best-fitting" the model with experimental data.

The char fraction was obtained by direct measurement following a test, with judgment on final height, char depth, and volume shrinkage of the sample. Janssens [26] gives data for the thermal conductivity of a typical dry wood at given densities and the variation in the thermal conductivity of char. From these data it can be shown that the ratio of the thermal conductivity of the virgin wood with the thermal conductivity of the char can be approximated to the ratio of the virgin wood density to the char density such that

$$\frac{k_\phi}{k_w} \approx \frac{\rho_\phi}{\rho_w} = \phi. \quad (55)$$

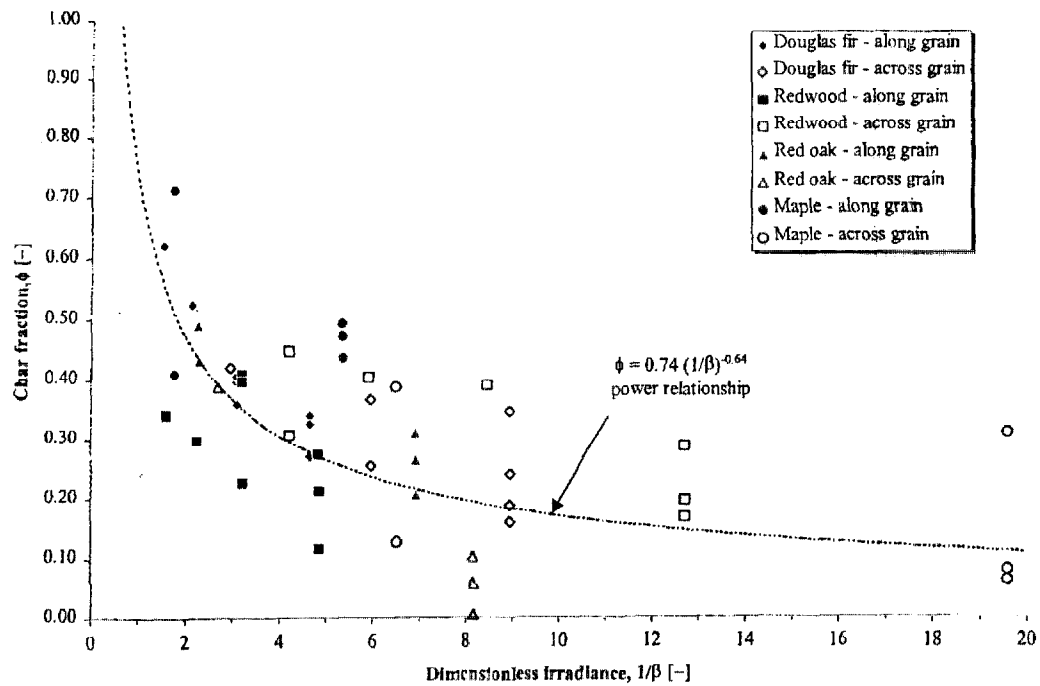


Fig. 7. Char fraction against dimensionless irradiance.

## ANALYSIS

### Char Fraction

A plot of measured char fraction against dimensionless irradiance is shown in Fig. 7 where the critical heat flux values used to obtain the dimensionless irradiance are derived from the integral model and shown in Table 1. A power curve fit gives the "best" trend for these data as

$$\phi = 0.74 \left( \frac{\dot{q}_i''}{\dot{q}_{cr}''} \right)^{-0.64} \quad (56)$$

There is a fair degree of scatter of the data that may partly be due to the difficulties of measuring the char depth. Clearly, this relationship may not be universal and only shows the "bulk" effects of heat flux on overall charring. Lyon [27] finds that the local char fraction of polymers is a function of temperature. In contrast, our char fraction is a bulk property resulting from a graduation of wood decomposition as well as char consumption due to oxidation.

### Determination of Flame Heat Flux and Heat of Gasification

For each species of wood at a given orientation, single values for the flame heat flux and the heat of gasification were selected such that the following were achieved:

- i. The short-time solution gave a reasonable match with the initial mass loss rate at ignition;
- ii. The intersection of the short-time and long-time solutions was comparable with the peak experimental burning rate;
- iii. The long-time solution followed the decay portion of the experimental burning rate.

It was found that adjusting the flame heat flux and heat of gasification to exactly match any one of the three criteria resulted in a poor comparison with the remaining two. Thus the selection of the flame heat flux and heat of gasification was based on obtaining a reasonable match with each of the three criteria. Once determined,

TABLE 2  
Heat of Gasification per Unit Mass of Virgin Wood and Flame Heat Flux Obtained  
from Iterative Analysis

Species	Grain Orientation	Derived Heat of Gasification $L$ (kJ/g)	Derived Flame Heat Flux $\dot{q}_f''$ (kW/m <sup>2</sup> )	Measured Average Flame Heat Flux, Hopkins [19] $\dot{q}_f''$ (kW/m <sup>2</sup> )
Redwood	<i>along</i>	2.8	35	44
	<i>across</i>	3.2	33	
Red oak	<i>along</i>	2.3	35	42
	<i>across</i>	2.3	33	
Douglas fir	<i>along</i>	1.6	17	
	<i>across</i>	2.9	46	
Maple	<i>along</i>	1.7	16	
	<i>across</i>	3.5	36	

these values were used over the range of radiant heating conditions of 25 to 75 kW/m<sup>2</sup>.

Clearly the values of the flame heat flux and heat of gasification obtained in this study are not intended to be exact for a particular species of wood at a given orientation. The iterative process and the need to arbitrarily decide what constituted a good match means that the values given here are only representative. Table 2 shows the final derived values for the heat of gasification and flame heat flux for each wood in the two grain orientations.

#### Comparisons Between Experiments and Theory

##### Burning Rate

The dimensionless equations for the burning rate are a relatively complex set of functions of several variables. In order to examine how each variable contributes to the behavior of the model, we can select a set of typical values for these variables and then vary any one over a range of values. To obtain the theoretical solutions, the analysis used the following properties and relationships: the heat of gasification and flame heat flux derived from the iterative approach given in Table 2; the characteristic material properties given in Table 1; and the char fraction relationship described by Eq. 56.

For example, Fig. 8 shows the variation in the theoretical burning rate with incident heat flux  $\dot{q}_i''$  taking typical values for Douglas fir in the *along* grain orientation. Figure 8 also plots the

average measured burning rate at each given incident heat flux from eight Douglas fir, *along* grain orientation tests so as to obtain the general form of the experimental data. Comparison with the theoretical solutions shows how the experimental data qualitatively compare with the integral model solutions. The peak dimensionless burning rate at low heat fluxes is greater than at high heat fluxes in both cases. The relative offset in the peaks as a function of time shown by the theory is more difficult to identify in the experimental data. In both the theoretical and experimental cases, at long times the burning rates at the various heat fluxes run parallel at a slowly decaying ( $1/\sqrt{t}$  as shown by Eq. 54) value although there is some minor fluctuation in the experimental data. Similar results were obtained for the other wood species and orientations tested.

Figure 9 shows typical measured burning rate and theoretical solutions for four samples. In order to clearly identify the growth and decay phases, only the first 600 seconds of each test are plotted. The theoretical solutions qualitatively compare well with the measured data. In most cases the transition from the short-time to the long-time solutions matches the time to the measured peak burning rate, particularly at the higher incident heat fluxes. The decay in the burning rate predicted by the long-time solution is qualitatively similar although the model underpredicts the burning rate in the *along* grain configurations as we move further away from ignition.

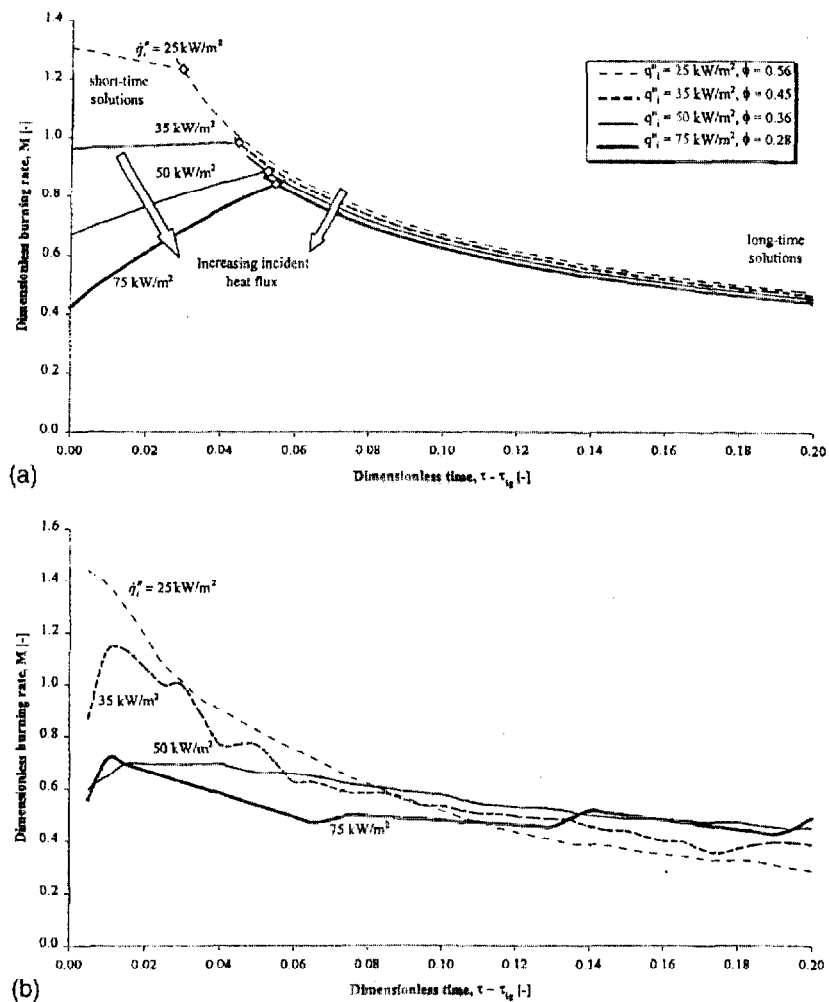


Fig. 8. Typical theoretical and experimental burning rate results. a) Theoretical burning rate solutions; b) Combined measured burning rates of Douglas fir in the *along* grain orientation using derived properties.

### Thermal Penetration Depth

Figure 10 shows typical theoretical thermal penetration depth solutions (derived from Eqs. 7, 50, and 51) compared with the thermocouple measurements. The experimental thermal penetration depth was mapped by obtaining the time at which each thermocouple recorded a rise of  $5^\circ\text{C}$  above the initial ambient temperature of the sample. The theoretical solutions compare well with the experimental data particularly at the shallower thermocouple depths, and this was found to be the case with almost all of the tests.

### Char Depth

The theoretical char depth is compared with the char depth obtained from Eq. 15 and the measured burning rate in Fig. 11 for four samples. The theoretical solutions to the integral model are qualitatively similar to the predicted char layer depth from the measured burning rate and compare well at  $75 \text{ kW/m}^2$ .

The char depths measured at the end of the tests were compared with the calculated char depth from Eq. 15 using the average mass loss rate measured in the Cone Calorimeter and  $t$  equal to the duration of the test  $t_f$  (Fig. 12). At

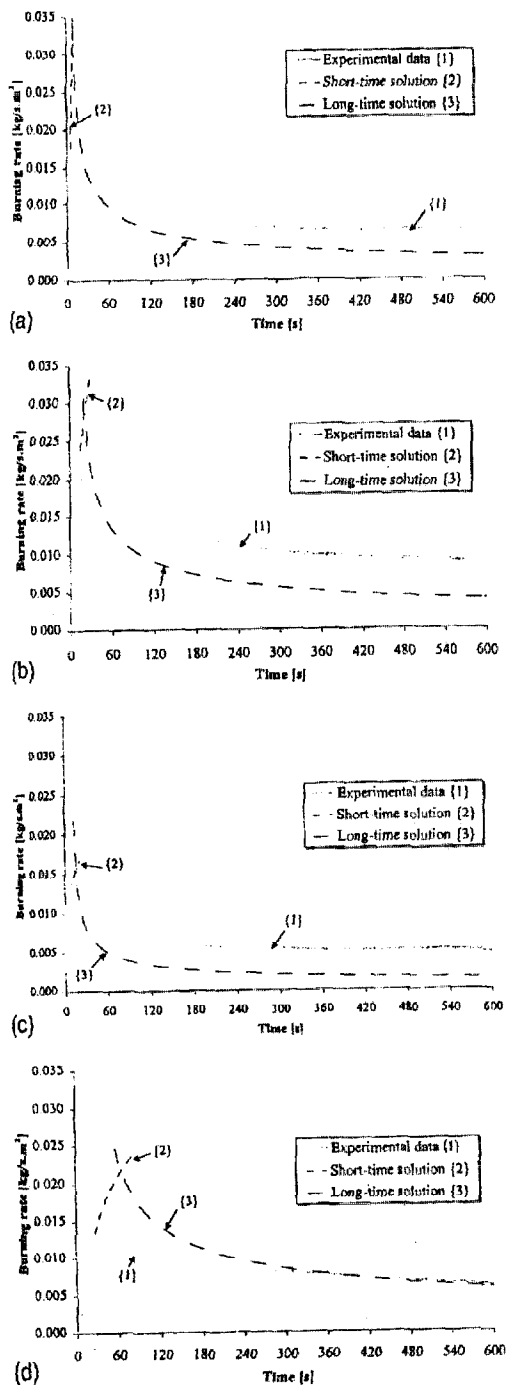


Fig. 9. Measured and theoretical burning rates. a) Douglas fir, along grain, 75 kW/m<sup>2</sup> for 25 mins; b) Red oak, along grain, 75 kW/m<sup>2</sup> for 25 mins; c) Redwood, along grain, 50 kW/m<sup>2</sup> for 25 mins; d) Maple, across grain, 75 kW/m<sup>2</sup> for 75 mins.

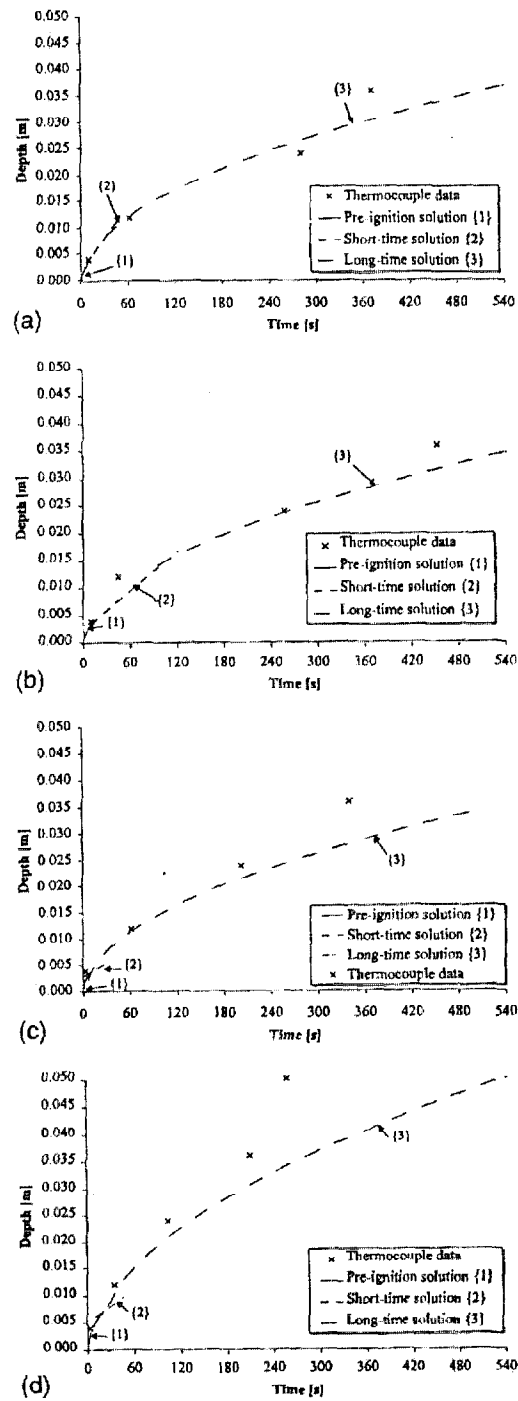


Fig. 10. Theoretical and measured thermal penetration depth. a) Douglas fir, along grain, 75 kW/m<sup>2</sup> for 25 mins; b) Red oak, along grain, 75 kW/m<sup>2</sup> for 25 mins; c) Redwood, along grain, 50 kW/m<sup>2</sup> for 25 mins; d) Maple, across grain, 75 kW/m<sup>2</sup> for 75 mins.

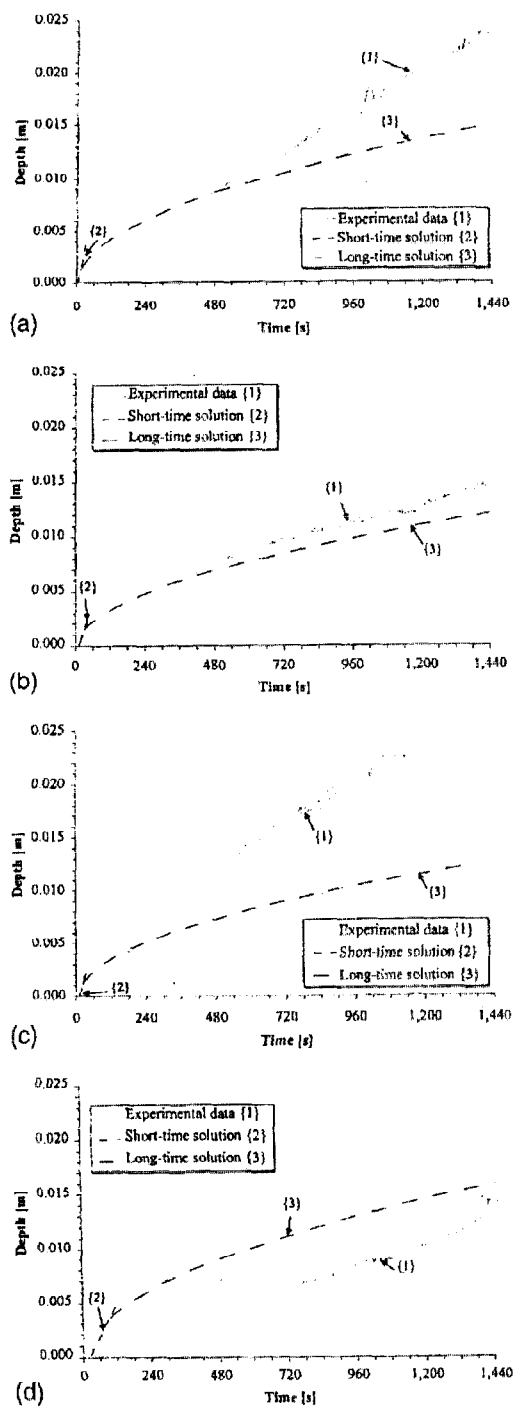


Fig. 11. Theoretical and measured char depth. a) Douglas fir, along grain, 75 kW/m<sup>2</sup> for 25 mins; b) Red oak, along grain, 75 kW/m<sup>2</sup> for 25 mins; c) Redwood, along grain, 50 kW/m<sup>2</sup> for 25 mins; d) Maple, across grain, 75 kW/m<sup>2</sup> for 25 mins.

earlier times (25 minutes), the calculated and measured data match fairly well though the mass loss rate relationship appears to overpredict slightly. However, at later times (75 minutes) the integral model fails to successfully predict the char depth compared with the measured data. It is likely that this is due to a back face effect; heat is lost through the back face and/or the sample is completely charred whereas the integral model treats the sample as having an infinite depth that can continue to char indefinitely.

### Char Oxidation

During the tests conducted it was observed that flaming would eventually cease and instead the char at the surface of the material would be oxidized away by the incident heat flux. The best example of this was shown by a test using Douglas fir, across grain orientation exposed for 75 minutes at 75 kW/m<sup>2</sup> where the rate of heat release and heat of combustion data clearly show the transition from wood burning to char oxidation (Fig. 13). The char oxidation mechanism is not included in the model used in this study.

The average heat of combustion during the flaming portion of the test was 9.2 MJ/kg for Douglas fir, which is comparable to the typical value of 10 MJ/kg expected from burning wood in the Cone Calorimeter as discussed in the "Introduction." The heat of combustion data exhibits a higher degree of fluctuation during the char oxidation phase due to the relatively low instantaneous mass loss rates. By taking an average of the heat of combustion during the char oxidation stage of the test, the heat of combustion of the char was found to be 35.5 MJ/kg. This value is higher than the 32 MJ/kg quoted by Janssens [3] but compares well with the average heat of combustion for char of 34.3 MJ/kg quoted by Roberts [28]. By using the average heat of combustion for char and the measured rates of heat release, the average "burning" rate of the char was found to be 0.0015 kg/s · m<sup>2</sup>.

Figure 13 also clearly shows the back effect, where the burning rate of the sample increases as the thermal wave is reflected at the rear of the sample. This is also not included in the

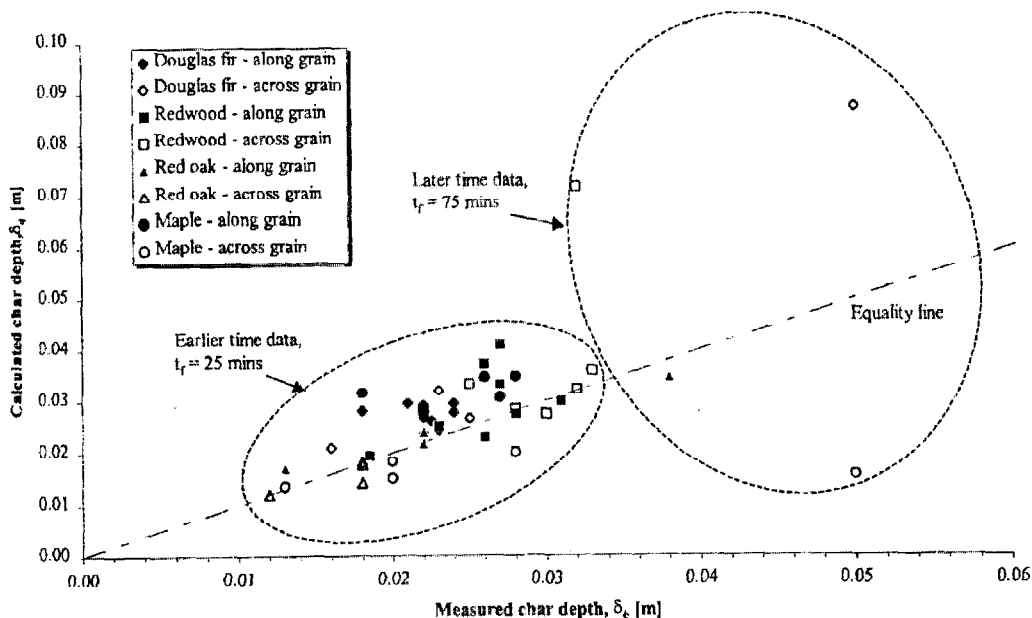


Fig. 12. Comparison of measured and calculated char depth.

model used here but was included in the integral model demonstrated by Moghtaderi et al. [21]. The solution to our integral model suggests that the thermal penetration wave reaches the back of the sample after approximately 1000 seconds, which compares well with the results presented in Fig. 13.

#### Maximum Surface Temperature

If it is assumed that after a "long" time the maximum temperature recorded by the topmost thermocouple is equivalent to the surface temperature (i.e., the surface and the wood or char at a depth of 4 mm are at equilibrium), then the experimental data and Eq. 52 can be compared. If it is assumed that the flame heat flux at long time is actually negligible i.e.,  $\dot{q}_f'' \approx 0$ , then Eq. 52 simply becomes

$$T_s \approx \left( \frac{\dot{q}_i''}{\sigma} \right)^{1/4} \quad (57)$$

and thus this gives an estimate of the minimum long-time surface temperature. Figure 14 shows an example of the measured maximum temperatures and the theoretical values from Eqs. 52 and 57 for redwood.

#### SUMMARY AND CONCLUSIONS

We have developed a theoretical model for the burning rate of wood and compared the solutions to that model with experimental data. We summarize the following:

1. The burning rate of wood depends on many factors, including the species, grain orientation, moisture content, exposure conditions, and the inherent variability of wood as a natural material.
2. After ignition, the integral model for the burning rate of a charring material can be expressed as a short-time and a long-time solution.
3. Effective heats of gasification based on the original wood mass were found to be about 1.5–3.0 kJ/g along the grain and 2.5–3.5 kJ/g across the grain.
4. The overall char fraction of wood has been found to be an inverse function of the ratio of the incident heat flux and the critical heat flux. The function may not be universal for all charring materials or even all species of wood.
5. Reasonable and experimentally plausible

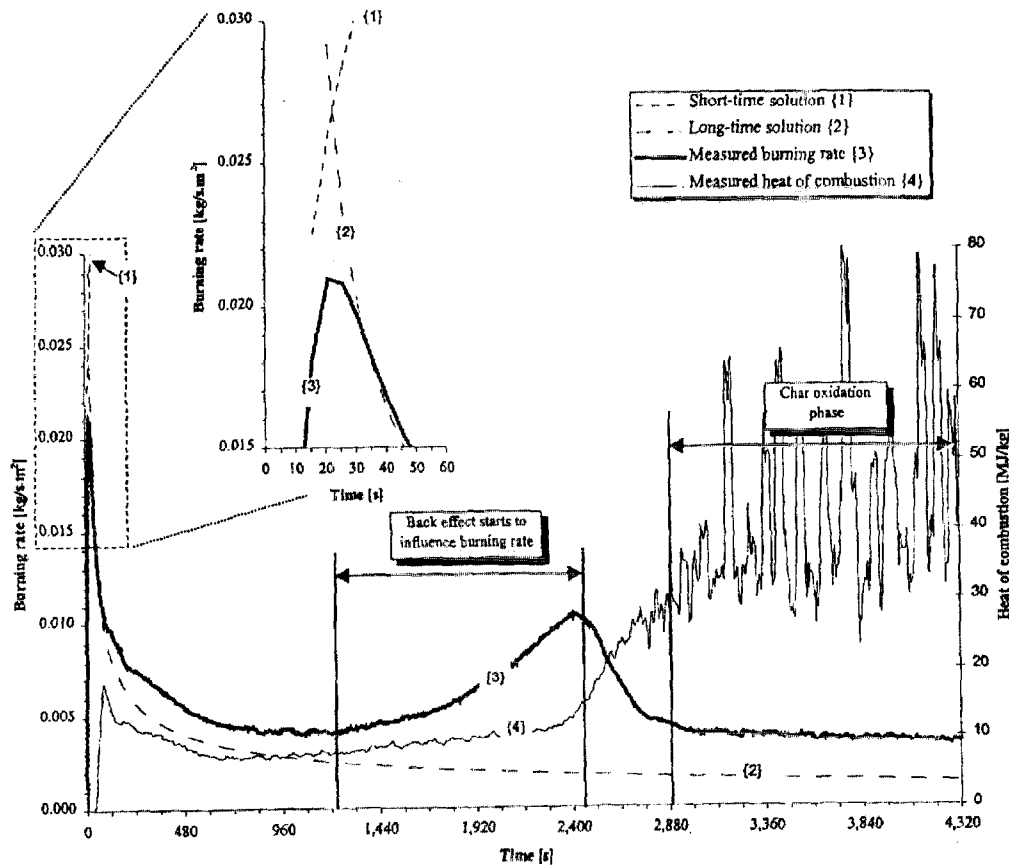


Fig. 13. Rate of heat release and heat of combustion for Douglas fir, across grain orientation exposed for 75 minutes at 75 kW/m<sup>2</sup> showing back effect and char oxidation phases.

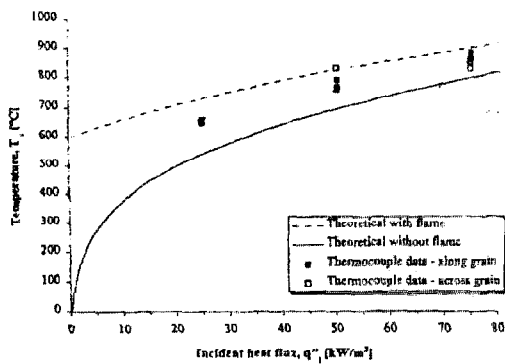


Fig. 14. Comparison between maximum theoretical and measured surface temperatures for redwood.

properties have been derived. The integral model's solutions for the burning rate qualitatively compare well with the measured data. The model predicts both the initial growth and the subsequent decay.

6. Thermocouples embedded into a burning sample can be used to estimate the thermal penetration depth and the surface temperature after a long time. Comparison between the thermocouple data and the integral model shows reasonable agreement for both parameters.
7. Prediction of the char depth can be made using the measured burning rate. The predic-

tions of char depth based on the measured mass loss rate and the measured char depth after an exposure of 25 minutes compare well. For an exposure of 75 minutes, the match is poor; this may be due to the finite thickness of the samples.

*The authors thank Robert Schroeder for allowing the additional data obtained on behalf of his studies to be used for this analysis and for his provision of extra test samples. The authors also note the partial support given by the Department of Fire Protection Engineering, University of Maryland and NIST/BFRL.*

## REFERENCES

1. Spearpoint, M. J. (1999). *Predicting the Ignition and Burning Rate of Wood in the Cone Calorimeter Using an Integral Model*. NIST-GCR-99-977, National Institute of Standards and Technology, Gaithersburg, MD.
2. *Standard Test Method for Heat and Visible Smoke Release Rates for Materials and Products Using an Oxygen Consumption Calorimeter*. (1995) NFPA 264, National Fire Protection Association, Quincy, MA.
3. Janssens, M. (1991). Ph.D. thesis, University of Gent, Belgium.
4. Drysdale, D. (1996). *An Introduction to Fire Dynamics*, John Wiley & Sons, Chichester.
5. Kanury, A. M., in *SFPE Handbook of Fire Protection Engineering*, 2nd ed., Society of Fire Protection Engineers, Boston, MA, 1995, pp. 2-190-2-204.
6. Roberts, A. F., *Combust. Flame* 14:261-272 (1970).
7. Simms, D. L., *Combust. Flame* 6:303-318 (1962).
8. Kanury, A. M. (1972). *Rate of charring combustion in a fire*. Proceedings of the Fourteenth Symposium (International) on Combustion, Pennsylvania State University.
9. Suuberg, E. M., Milosavljevic, I., and Lilly, W. D. (1994). *Behavior of Charring Materials in Simulated Fire Environments*. NIST-GCR-94-645, National Institute of Standards and Technology, Gaithersburg, MD.
10. Atreya, A. (1983). Ph.D. thesis, Harvard University, Cambridge, MA.
11. Atreya, A., Carpentier, C., and Harkleroad, M. *Effect of sample orientation on piloted ignition and flame spread*. Fire Safety Science—Proceedings of the First International Symposium, pp. 97-109. Hemisphere Publishing Corp., NY 1986.
12. Chen, Y., Delichatsios, M. A., and Motevalli, V., *Combust. Sci. Technol.* 88:309-328 (1993).
13. Wichman, I. S., and Atreya, A. *Combust. Flame* 68: 231-247 (1987).
14. Yuen, R., Casey, R., De Vahl Davis, G., Leonardi, E., Yeoh, G. H., Chandrasekaran, V., and Grubits, S. J. in *Fire Safety Science. Proceedings. Fifth International Symposium, Melbourne, Australia* (Y. Haseemi, Ed.), International Association for Fire Safety Science, Boston, MA, 1997, pp. 189-200.
15. Parker, W. J. *Prediction of the heat release rate of wood*. Fire Safety Science—Proceedings of the First International Symposium, pp. 207-216. Hemisphere Publishing Corp., NY, 1986.
16. Quintiere, J. G. (1992) *A Semi-Quantitative Model for the Burning Rate of Solid Materials*. NISTIR 4840, National Institute of Standards and Technology, Gaithersburg, MD.
17. Quintiere, J. G., and Iqbal, N., *Fire Mater.* 18:89-98 (1994).
18. Anderson, G. W. (1997). *A Burning Rate Model for Charring Materials*. NIST-GCR-97-725, National Institute of Standards and Technology, Gaithersburg, MD.
19. Hopkins, D. (1995). *Predicting the Ignition Time and Burning Rate of Thermoplastics in the Cone Calorimeter*. NIST-GCR-95-677, National Institute of Standards and Technology, Gaithersburg, MD.
20. Hopkins, D., and Quintiere, J. G., *Fire Safety J.* 26:241-268 (1996).
21. Moghtaderi, B., Novozhilov, V., Fletcher, D., and Kent, J. H., *Fire Mater.* 21:7-16 (1997).
22. Schroeder, R. A. (1999). Doctor of engineering dissertation, University of California, Berkeley.
23. Rhodes, B. T., and Quintiere, J. G., *Fire Safety J.* 26:221-240 (1996).
24. Siegel, R., and Howell, J. R., *Thermal Radiation Heat Transfer*, 2nd ed., Hemisphere Publishing Corp., Washington, D.C., 1981.
25. Tran, H. C., and White, R. H., *Fire Mater.* 16:197-206 (1992).
26. Janssens, M. L. Proceedings of the Pacific Timber Engineering Conference, Gold Coast, Australia, pp. 607-618, 1994.
27. Lyon, R. E., *Solid-State Thermochemistry of Flaming Combustion*, Federal Aviation Administration, Atlantic City, NJ, 1999.
28. Roberts, A. F., *Combust. Flame* 8:245-246 (1964).

*Received 3 August 1999; revised 3 February 2000, accepted 10 May 2000*